Biosensors and Bioelectronics 144 (2019) 111667

Contents lists available at ScienceDirect

Biosensors and Bioelectronics

journal homepage: www.elsevier.com/locate/bios

QCM based enantioselective discrimination of enantiomers by a pair of serine derived homochiral coordination polymers

Ming-Hua Xie, Feng Cheng, Ya Wang, Bai-Xin Yao, Wei Wang, Rong-Feng Guan, Xiu-Li Yang*

Key Laboratory for Advanced Technology in Environmental Protection of Jiangsu Province, Yancheng Institute of Technology, Yancheng, 224051, PR China

ARTICLE INFO

Keywords:
Amino acid
Homochiral coordination polymer
Enantioselective sensor
Quartz crystal microbalance

ABSTRACT

Decoding enantioselective molecular interactions between sensors and guests into readable signal represents a great challenge in developing selective sensing technology. In this work, a pair of serine derivatives based homochiral coordination polymer (HCP) enantiomers, (L)-SA-Cd and (D)-SA-Cd, were synthesized and explored as enantioselective sensors towards guest enantiomers. Quartz crystal microbalance (QCM) technology was employed to indicate the gravimetric change of (L)- and (D)-SA-Cd towards variable chiral guests, and an enantioselective factor of 1.72 ± 0.15, 1.81 ± 0.08, 1.37 ± 0.03 and 2.89 ± 0.09 were achieved for lactic acid, menthol, valinol and 1-phenylethylamine (PEA), respectively. PEA was further selected to comprehensively study the enantioselectivity via electrochemical tests, HPLC analysis and theoretical calculations. By comparison with state-of-art works, the enantioselective discrimination for PEA enantiomers is better than a vast majority of similar reports. (L)- and (D)-form of SA-Cd exhibited mirror behaviors towards guest enantiomers, and control experiments indicated the role of HCP construction in enhancing enantioselectivity. H-bonding effect was found to be the binding force between SA-Cd and PEA, as verified by FT-IR and UV–Vis titration studies. Further DFT calculations revealed the existence of conformation oriented H-bonding between the chiral –OH groups of serine fragment and $–NH_2$ group of PEA. The findings indicate that HCP construction represents an effective strategy for promoting enantioselectivity, and monitoring gravimetric change could be a promising general method in decoding most of the enantioselective recognition process.

1. Introduction

Chirality is an essential feature of life, and the study of chirality has been playing a significant role in medical diagnosis, pharmacology and organic synthesis, etc (Kumar and Liz-Marzán, 2019; Liu et al., 2016; Morris and Bu, 2010; Zuo et al., 2016). Enantioselective recognition is one of the major research topics of modern chiral science, and growing efforts have been devoted to the development of enantioselective recognition technologies (Ma et al., 2019; Martell et al., 2017; Sethy et al., 2017; Staszak et al., 2019; Zhang et al., 2016). Enantioselective recognition reveals the molecular interactions between enantiomers and provides key information for understanding and tuning asymmetric catalysis. However, many recognition process accompanied by no significant change of properties, and the short of a general method to decode the recognition into simple readable signal represents a great barrier in realizing enantioselective sensing (You et al., 2015). Mass is an essential feature of object, and in many research fields, such as physics and biology, the change of mass is widely used to index the status of target system. Similarly in chemical sensing areas, the selective interaction between a sensor and a guest may also cause significant gravimetric change of the sensing system. Compared with other popular decoding strategies such as fluorescence, UV and circular dichroism (CD), which could only be used in specific sensing system, gravimetric change takes the advantage of being much more general and the fabrication of mass-based decoding system represents a promising solution to the realization of potential sensors (Chankvetadze, 2004; Jensen et al., 2008; Pu, 2012; Zhao et al., 2017).

Homochiral metal-organic frameworks (HMOFs) have gained growing interests for their promising applications in chiral separation, enantioselective recognition as well as asymmetric catalysis (Cui et al., 2016; Ma et al., 2009; Pan et al., 2019; Slater et al., 2017). It should be noticed that the construction of HMOFs still represents a great challenge. On the contrary, constructing non-porous homochiral coordination polymers (HCPs) could greatly lower the synthetic barrier, and the employment of naturally abundant, low-cost product as the linkers could further advance the progress. Amino acids are a class of typical chiral natural molecules, and the free amino group could be readily derived by simple chemical reactions. Besides, the R-groups of amino

* Corresponding author.
E-mail address: xlychem@126.com (X.-L. Yang).

https://doi.org/10.1016/j.bios.2019.111667
Received 29 June 2019; Received in revised form 27 August 2019; Accepted 29 August 2019
Available online 31 August 2019
0956-5663/

acid could further provide multi-functionalities, making them ideal candidates in constructing HCPs (Mon et al., 2017; Yang et al., 2011a, 2011b, 2014; Yoshinari and Konno, 2018). Herein, we report a pair of serine derived HCP enantiomers (L)-SA-Cd and (D)-SA-Cd, which were fabricated into enantioselective QCM sensors for various guest enantiomers. SA-Cd exhibited the highest selectivity towards 1-phenylethylamine (PEA) with an enantioselective factor of 2.89 ± 0.09. Density Functional Theory (DFT) calculations along with control experiments all indicate that chiral conformation orientated H-bonding should be responsible for the observed enantioselectivity.

2. Experimental section

2.1. Synthesis of SA-Cd enantiomers

All chemicals were commercially available and were used without further purification, except the chiral ligands (L)- and (D)-4-(serine) methyl-benzoic acid ((L)- and (D)-H_2SA) were synthesized according to literature method (Yang et al., 2011b). Heating a mixture of Cd $(ClO_4)_2{\cdot}6H_2O$ (8.4 mg, 0.02 mmol), (L)-H_2SA (2.4 mg, 0.01 mmol) and NaOH (8 drops, 0.05 M) in a mixed solvent of DMF (1 mL) and H_2O (1 mL) at 95 °C yielded colorless pillar crystals of (L)-SA-Cd after 24 h, which were filtered, washed with H_2O, EtOH and Et_2O, and dried at room temperature. Yield: 81% based on ligand. (D)-SA-Cd could be readily collected by using (D)-H_2SA as the ligand following otherwise same procedures. CCDC 1823030, 1916277 contain the crystallographic data for this paper.

2.2. Structural analysis

The crystal structure was solved by direct methods, and refined by full-matrix least-square methods with the SHELX-97 program package. Due to the highly localized electronic states of SA-Cd caused by the $3d^{10}$ configuration of Cd(II), idealized non-periodic clusters of [(L)-$SA_2Cd_2(H_2O)_4$] and [(D)-$SA_2Cd_2(H_2O)_4$] were built upon the single crystal data as the representative of (L)- and (D)-SA-Cd for theoretical studies using Gaussian 09 package (Frisch, et al., 2013; Pramanik et al., 2011; Yi et al., 2015). B3LYP together with the 6-31G basis set for C, H, O, N and LANL2DZ basis set for Cd were chosen for the structure optimization and energy calculation. Further periodical calculations were performed using the Perdew-Burke-Ernzerhof (GGA-PBE) (Perdew et al., 1992) exchange-correlation functional implemented in the plane-wave based Vienna ab initio simulation package (VASP) (Kresse and Furthmüller, 1996), the projector augmented wave (PAW) method (White and Bird, 1994) with a frozen-core approximation was used to describe the ion-electron interactions. A cutoff energy of 400 eV and the conjugate-gradient algorithm were used in the calculations. A 1×1 supercell with one layer was used to mimic the (001) surfaces of (L)- and (D)-SA-Cd, respectively. The slabs were separated by vacuums of 15 Å. All calculations were carried out in the National Supercomputing Center in Shenzhen, China.

2.3. QCM setup for enantioselective sensing

Freshly prepared (L)-SA-Cd was finely ground and sonicated in iso-propanol for 1 h prior to use (1 mg/mL). The well dispersed (L)-SA-Cd was spin-coated onto a 5 MHz AT-cut QCM crystal with 1 inch diameter Au electrode. Iso-propanol was removed under vacuum, and the coated crystal pallet was placed in a flow cell adapter connected to an SRS QCM-200 quartz crystal microbalance. A three-way valve connected to a N_2 gas flow (0.2 mL/min) was used to deliver the analyte vapour into the sensing adaptor. QCM results for (D)-SA-Cd were collected following identical procedures. For reproducibility test, after each run of test the SA-Cd coated QCM crystal was immersed in absolute EtOH for 6 h followed by washing with EtOH (10 mL × 3) to remove any adsorbed PEA, and then dried in vacuum at 75 °C overnight to regenerate.

According to the Sauerbrey equation, the gravimetric change (Δm) on the surface of quartz crystal is related to the shift in resonance frequency (Δf):

$$\Delta f = -\frac{2nf_0^2}{\sqrt{\rho_q \mu_q}} \times \Delta m = -C_f \times \Delta m \quad (1)$$

where

n = number of the harmonic at which the crystal is driven,
f_o = the resonant frequency of the fundamental mode of the crystal in Hz,
ρ_q = density of quartz = 2.648 g cm^{-3},
μ_q = shear modulus of quartz = 2.947×10^{11} g $cm^{-1}{\cdot}s^{-2}$.
C_f is called the sensitivity factor for the crystal, and in this study the value of C_f is 56.6 Hzμg^{-1}cm^2.

2.4. Electrochemical studies

(L)- or (D)-SA-Cd coated glassy carbon electrode was used as the work electrode, with Pt wires as the auxiliary and referential electrodes. The coating was performed in the presentence of Nafion, typically, 0.5 mg of sample was ground with 1 mL of EtOH and 20 μL of Nafion solution for 30 min. The resulting mixture was carefully drop-casted onto the pre-cleaned glassy carbon electrode and dried at room temperature thoroughly. The electrochemical response were performed in anhydrous CH_3CN with 0.01 M TBAP ($[(n\text{-}Bu)_4N]PF_6$) acting as the supporting electrolyte, and a bias of 0.5 V was applied.

2.5. Typical procedure for enantioselective adsorption of racemic PEA

0.05 mmol of (L)-SA-Cd was mixed with a hexane solution of racemic PEA (0.005 M, 1 mL), and the mixture was left standing in dark overnight. The upper clear solution was then subjected to chiral HPLC analysis. (L)-serine, (D)-serine, (L)-H_2SA, (D)-H_2SA and (D)-SA-Cd were studied under identical conditions.

3. Results and discussion

Solvothermal self-assembly of (L)- and (D)-H_2SA with Cd(II) in DMF/H_2O yielded two HCP enantiomers of (L)-SA-Cd and (D)-SA-Cd, respectively. The two HCPs adopt similar coordination motifs, and (L)-SA-Cd is selected for further structural discussion. (L)-SA-Cd crystallized in the monoclinic $P2_1$ space group with one (L)-SA ligand, one Cd (II) atom and two coordinated H_2O molecules in the fundamental asymmetric unit. Each Cd(II) atom is surrounded by one nitrogen atom and six oxygen atoms coming from two different water molecules and two (L)-H_2SA ligand molecules (Fig. 1a), each (L)-SA coordinates to two different Cd(II) atoms forming a 1D left-handed helical chain (Fig. 1b and S1). Different helical chains are interconnected via H-bonds, forming a stacking 3D structure (Fig. S3). It should be noticed that the conformation of –NH– group is fixed upon coordinating to a Cd(II) atom, and the loss of free molecular rotatory indicating that the –NH– group should be considered as a new emerging chiral centre (Yang et al., 2011a). (D)-SA-Cd follows the same coordination motif (Fig. 1c and S2), and a mirror structure of right-handed helical chain is found (Fig. 1d and S4). The enantiomeric nature could be verified by comparing the solid-state CD spectra of the ligands and frameworks, and mirror images could be found in the range of 200–800 nm (Fig. 1e). Except for CD spectra, TG curves (Figs. S7 and S8) and FT-IR spectra (Figs. S9 and S10) of the two enantiomeric frameworks give almost identical results. Due to the formation of complicated H-bonds between different helical chains, no accessible free space could be found in SA-Cd, and only the loss of two coordinated H_2O molecules could be found in TG curves. Although a condensed structure, which is usually considered as an unfavourable prototype for developing sensors, is resulted

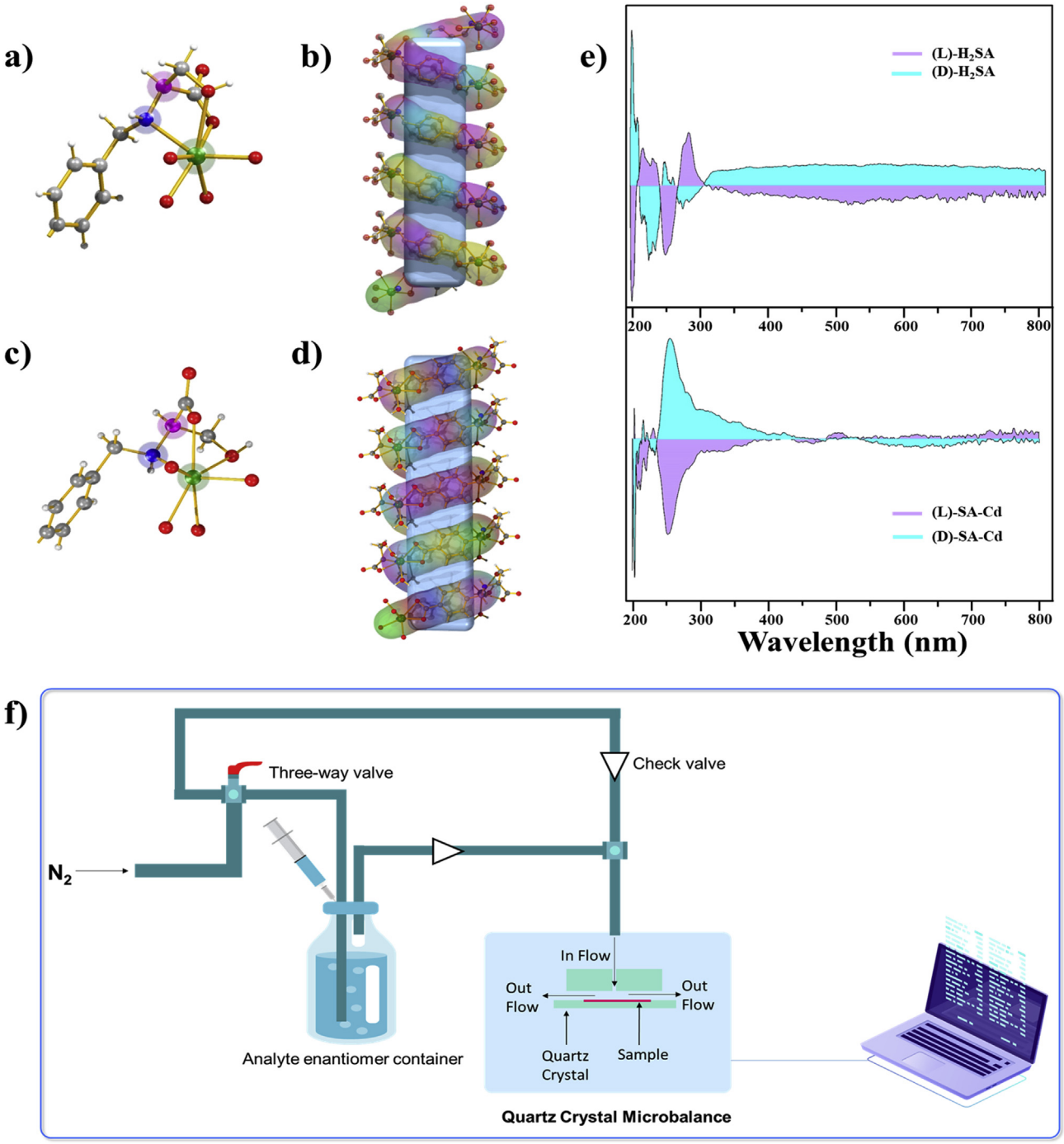

Fig. 1. Illustration of the structural features in SA-Cd. a) local coordination environment of Cd(II) in (L)-SA-Cd; b) 1D left-handed helical chain in (L)-SA-Cd; c) local coordination environment of Cd(II) in (D)-SA-Cd; d) 1D right-handed helical chain in (D)-SA-Cd; e) solid-state CD spectra of (L)- and (D)-form of ligands and frameworks; f) illustration of the setup for QCM sensing of enantiomers.

due to the complicated H-bonding effect, the dynamic disassociation nature of H-bonds offers a potential effective way in developing enantioselective applications (Mahadevi and Sastry, 2016).

As observed from the Single-X ray diffraction analysis, the free access space located inside the two polymers is quite limited, and N_2 adsorption/desorption tests were performed at 77K to further verify this. The two frameworks exhibited a type II isotherm, indicating the nonporous nature, and BET surface areas for (L)-SA-Cd and (D)-SA-Cd are calculated to be 5.74 and 6.33 $m^2 g^{-1}$, respectively. Given the poor BET surface areas of SA-Cd enantiomers (Fig. S11), it is wiser to reduce the dimension of bulk materials so that a better host-guest interactions could be achieved. Motivated by the recent progress, thin film devices of the two HCP enantiomers were prepared (Figs. S12–S14) and their enantioselective recognition behaviours were further investigated by QCM technology (Heinke and Wöll, 2019), using a gas-phase QCM sensing setup as schematically depicted in Fig. 1f. Four pairs of volatile bioactive enantiomers, (D)- and (L)-lactic acid, (D)- and (L)-menthol, (D)- and (L)-valinol, (D)- and(L)-PEA were selected to evaluate the enantioselectivity of SA-Cd. The QCM results are plotted in Fig. 2 and Figs. S15–S20, and the data is summarized in Table 1.

Upon exposing to different enantiomer vapors, the frequency of the fabricated thin film was significantly decreased, indicating the increase

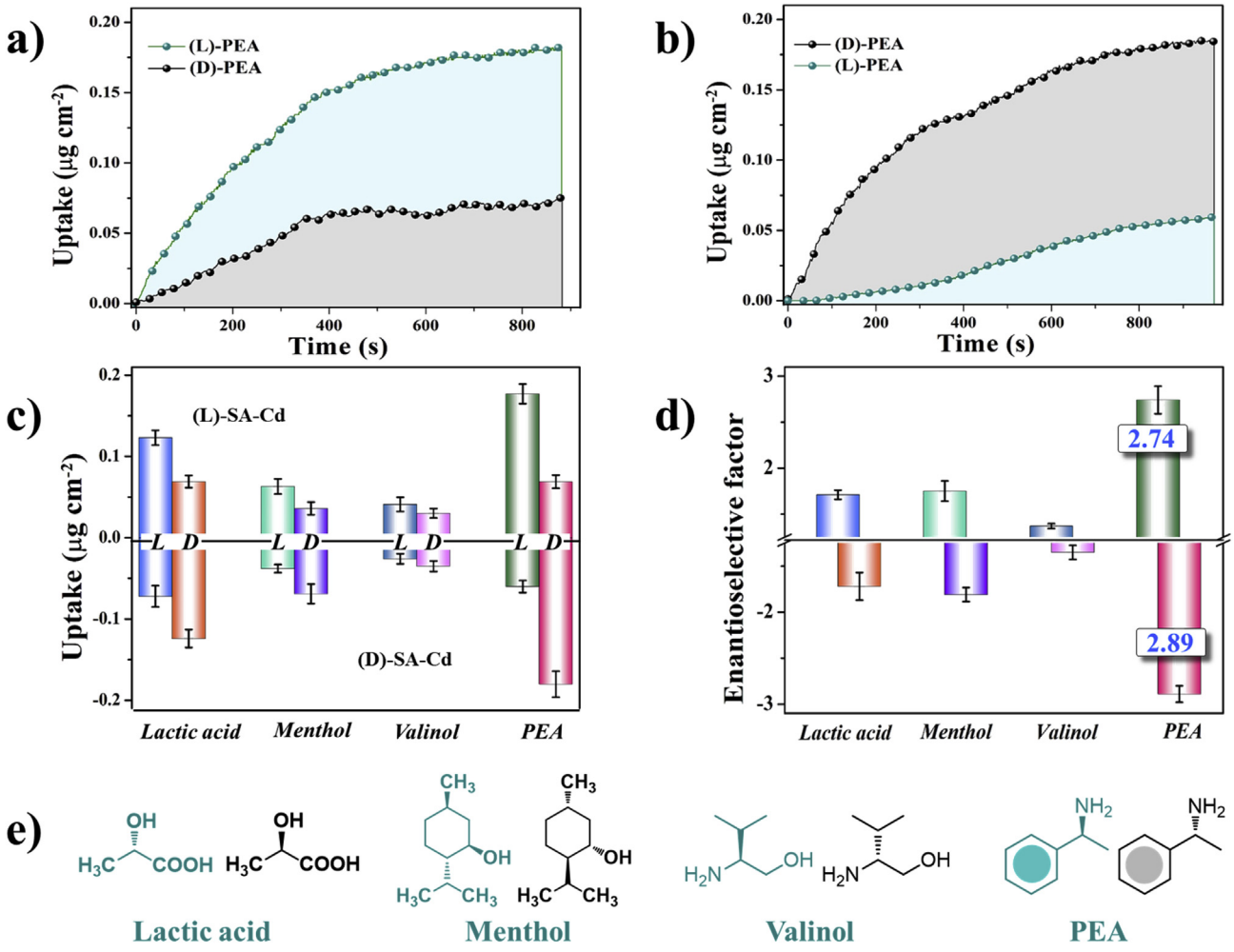

Fig. 2. QCM sensing results of SA-Cd enantiomers. a) PEA enantiomers uptake of (L)-SA-Cd; b) PEA enantiomers uptake of (D)-SA-Cd; c) comparison of the uptake of four enantiomeric guests by (L)-SA-Cd and (D)-SA-Cd; d) comparison of the *ef* value calculated from the different mass uptake of enantiomers; e) chemical structures of enantiomeric guests used in this study, the (L)- and (D)-form are marked with cyan and black, respectively. (For interpretation of the references to color in this figure legend, the reader is referred to the Web version of this article.)

of mass. The mass increase, i.e. the uptake of the enantiomeric guest, was calculated according to equation (1). (L)-SA-Cd and (D)-SA-Cd exhibited guest dependent mass uptake, and the selective uptake values between (L)- and (D)- form of analyte indicate the corresponding enantioselectivity. According to the most popular way of calculating enantioselectivity (Dong et al., 2017; Wanderley et al., 2012) and considering the particularity of gravimetric sensing (i.e. initial signal value is 0), the enantioselective factor (*ef*) of (L)-SA-Cd enantiomer for different enantiomeric guests could be calculated based on the following simplified equation (2):

$$ef_L = \frac{m_L - m_i}{m_D - m_i} = \frac{m_L}{m_D} \times 100\% \quad (2)$$

Where ef_L denotes the enantioselective factor of (L)-SA-Cd enantiomer for (L)-form of analyte; m_i is the initial uptake value, which is 0 in gravimetric study; m_L and m_D are the uptake values of the (L)- and

Table 1
Mass uptake and enantioselectivity of SA-Cd enantiomers.

	(L)-SA-Cd		(D)-SA-Cd	
Enantiomeric Guest	Uptake (μg cm^{-2})	Enantioselectivity factor for (L)-form guest	Uptake (μg cm^{-2})	Enantioselectivity factor for (D)-form guest
(L)-lactic acid	0.123 ± 0.009	1.71 ± 0.05	0.072 ± 0.013	1.72 ± 0.15
(D)-lactic acid	0.072 ± 0.008		0.124 ± 0.011	
(L)-menthol	0.063 ± 0.009	1.75 ± 0.11	0.038 ± 0.005	1.81 ± 0.08
(D)-menthol	0.036 ± 0.008		0.069 ± 0.012	
(L)-valinol	0.041 ± 0.009	1.37 ± 0.03	0.026 ± 0.006	1.35 ± 0.08
(D)-valinol	0.030 ± 0.006		0.035 ± 0.007	
(L)-PEA	0.181 ± 0.012	2.74 ± 0.15	0.063 ± 0.008	2.89 ± 0.09
(D)-PEA	0.066 ± 0.008		0.182 ± 0.016	

(D)-form of guest, respectively. For the case of (D)-SA-Cd, the corresponding ef_D could be calculated using a similar equation.

The QCM results clearly indicate the enantioselectivity of SA-Cd, and (L)- and (D)-form of SA-Cd exhibited almost mirror uptake behaviors. Guest enantiomers of the same conformation with SA-Cd gave much higher mass uptake, i.e. (L)-SA-Cd preferentially adsorb (L)-form of enantiomers while (D)-SA-Cd preferentially adsorb (D)-form of enantiomers. The highest *ef* value is found for PEA, and the selective forming of H-bonds between the $–NH_2$ group of PEA and –OH group of SA-Cd should be the reason for the observed high enantioselectivity. Control experiments were carried out to verify the role of constructing HCPs in promoting the enantioselectivity (Figs. S21–S24, Table S2). H_2SA could uptake more PEA compared with SA-Cd due to its abundance in carboxylate groups, however the corresponding *ef* value is much lower, suggesting the effectiveness of polymer construction in enhancing enantioselectivity. Reproducibility tests indicated that SA-Cd coated crystal could be used for several times without losing enantioselectivity, and the decrease in uptake capacity may originate from the exfoliation of deposited thin film during recovery (Figs. S25–S28, Table S3).

Electrochemical tests were employed to give a new interpretation of the enantioselective behavior. As shown in Fig. 3a and b, due to the non-conductive nature of common coordination polymers, SA-Cd exhibited quite low electric current upon applying a bias. Subsequently, a certain amount of PEA enantiomer was carefully injected into the working electrolyte and let it diffused to the PEA modified electrode naturally. After several tens of seconds of PEA addition, a gradual enhancement in the electric current was observed, and an equilibrium was reached after about 40 min of PEA addition. Similar with that of QCM studies, the electrochemical response of SA-Cd exhibited typical enantioselectivity, a greater enhancement in electric current was found when a PEA enantiomer of the same conformation with that of SA-Cd was added, and an adequate enhancement was found when PEA enantiomer of the opposite conformation with that of SA-Cd was added. According to equation (2), (L)-SA-Cd exhibits an electrochemical *ef* of 2.67 ± 0.14 for (L)-PEA while (D)-SA-Cd exhibits 2.64 ± 0.16 for (D)-PEA. The reason for the electric current enhancement should be ascribed to the formation of additional H-bonds, which could provide effective proton transfer channel to give better conductivity and has been used as an effective tool to tune the conductivity of a framework (Meng et al., 2017; Yang et al., 2017; Zhang et al., 2017). Greater electric current enhancement suggests the formation of more H-bonds, i.e. preferential absorption of specific guest molecules. The *ef* values given by electrochemical test are in accordance with that of QCM studies, further confirming the enantioselectivity of SA-Cd towards PEA enantiomers.

Encouraged by the enantioselectivity of SA-Cd for single PEA enantiomer, racemic PEA was further used to evaluate the enantioselective absorption capability of SA-Cd. (L)- and (D)-form of serine, H_2SA and SA-Cd were used as the adsorbents, and the enantiomeric excess (*ee*) value of tested PEA solution was analyzed by chiral HPLC (Figs. S29–S35). The *ee* value is calculated according to equation (3):

$$ee = S_{(D)\text{-PEA}} - S_{(L)\text{-PEA}} \quad (3)$$

Where *ee* denotes the enantioselective excess value, $S_{(D)\text{-PEA}}$ and $S_{(L)\text{-PEA}}$ are the peak area percentages of (D)-PEA and (L)-PEA calculated

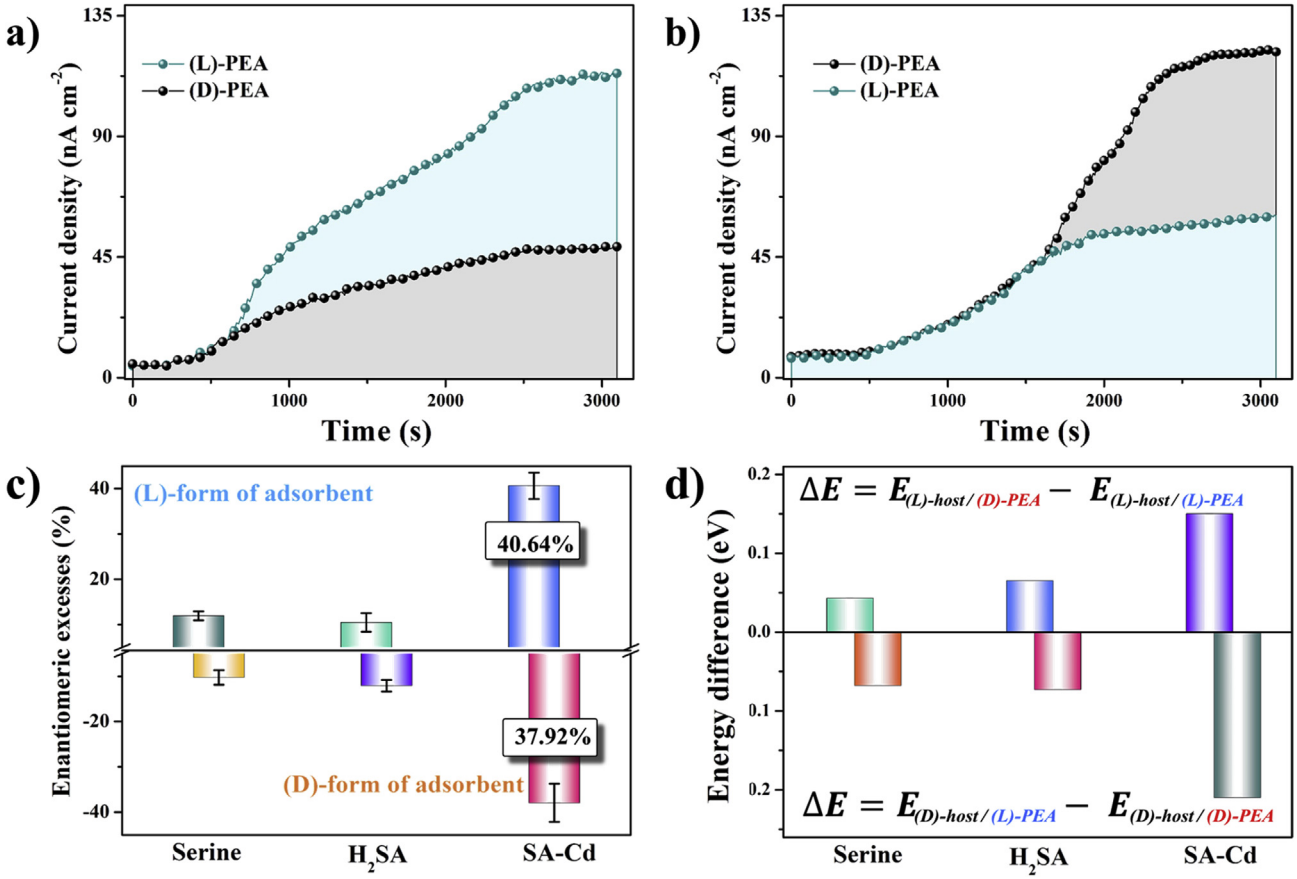

Fig. 3. Verification of the enantioselective activity of (L)- and (D)-SA-Cd. a) Time-dependent electrochemical response of PEA enantiomers over (L)-SA-Cd; b) Time-dependent electrochemical response of PEA enantiomers over (D)-SA-Cd; c) comparison of the *ee* values of original racemic PEA solution after adding (L)- and (D)-form of serine, H_2SA and SA-Cd as the adsorbents for 12 h; d) Calculated energy difference of the complexes formed by (L)- and (D)-form of serine, H_2SA, SA-Cd host and PEA enantiomers.

from chiral HPLC analysis, respectively. The *ee* values of PEA solution after being treated with different adsorbents are plotted in Fig. 3c. Same with that of QCM and electrochemical studies, (L)-form of adsorbent preferentially adsorbs (L)-PEA, leaving more (D)-PEA in the solution, and (D)-form of adsorbent exhibited mirror-like behaviors leaving more (L)-PEA in the solution. (L)-serine gave an *ee* value of 11.96 ± 0.97% while (D)-serine gave an *ee* value of −10.26 ± 1.62%, suggesting the enantioselective adsorption of serine. Similarly, H_2SA ligand gave comparable results with that of serine, and *ee* values of 10.48 ± 2.06% and −12.08 ± 1.29% were achieved for (L)- and (D)-H_2SA, respectively. Considering the similarity of molecular structures and the comparable *ee* values given by serine and H_2SA, the chiral serine fragment should be considered as the active sites for chiral adsorption.

Interestingly, SA-Cd gave much improved results and the *ee* values for (L)- and (D)-SA-Cd were 40.64 ± 2.91% and −37.92 ± 4.20%, respectively. The reason for the observed enhancement in enantioselectivty should be ascribed to the construction of coordination polymer, inside which the achiral benzoic groups are firmly fixed leaving only surface exposed chiral –OH groups to form H-bonds with PEA enantiomer. As a chiral molecule, PEA plays a great important role in biological and medical fields, and the small molecular size makes it difficult to achieve high enantioselectivity for PEA involved studies. By comparing literature results on PEA enantioselective recognition (Table 2), SA-Cd gives an *ef* value higher than 80% of reported values. Moreover, compared with all those involving racemic PEA studies, the *ee* value given by SA-Cd is better than a vast majority of literature results, the low-cost and facile synthetic procedures representing a significant progress in developing enantioselective probe for PEA enantiomers.

According to Single X-ray diffraction analysis, the formation of H-bonds should be the reason for the enantioseletivity as confirmed by comprehensive experimental studies. FT-IR spectra of the complexes formed by PEA enantiomers and chiral hosts were recorded to study the possible H-bonding effect (Figs. S36–S47, Table S4). Serine exhibited guest dependent variation both in the carboxylate and hydroxyl regions, suggesting the occurrence of potential chiral recognition. H_2SA exhibited the most significant changes among those studied cases, the stretching vibration of the benzoic acid group disappeared by forming H-bonds with PEA molecules while the absorption for –OH group remained unchanged, indicating a strong binding effect but with no contribution to enantioselectivity (Tables S2 and S7 and Scheme S1). For the case of SA-Cd, only the hydroxyl group exhibited significant and guest dependent shift to lower wavenumbers, indicating the formation of enantioselective H-bonds with PEA molecules. UV–Vis titration experiments were carried out to calculate the corresponding binding constants (K) using literature method (Anand et al., 2014; Table S5, Figs. S48–S59). The binding constants for each host exhibit similar enantioselectivity, larger binding constant value was obtained towards the guest with the same conformation with that of host. Interestingly, H_2SA ligand gave the largest K value, which is about 3 orders of magnitude larger than that of serine. However, the difference between K_L and K_D is small, indicating a poor enantioselectivity. According to the FT-IR tests, the benzoic acid group of H_2SA ligand should be the reason for the observed large binding constant, and such strong binding effect could make no contribution to the promotion of enantioselectivity due to the achiral nature of this group (Scheme S1, Table S7). SA-Cd gave adequate binding constant values with the largest difference between K_L and K_D, indicating the enantioselective binding effect towards chiral guest.

To further understand the enantioselective process, DFT calculations were performed and (L)-and (D)-form of serine, H_2L and SA-Cd were selected as the host to study their complexes formed with PEA enantiomers. Calculations indicate that all selected hosts could form complexes with PEA enantiomers via H-bonding between the chiral –OH group of serine and $–NH_2$ group of PEA. As shown in Figs. 3d and 4 and Figs. S60–S63, PEA enantiomer which shares the same conformation with that of host takes a more favorable spatial position approaching to the chiral –OH group, and a stable complex could be formed. For all studied cases, the total energy of the complex formed by (L)-host and (L)-PEA is much lower than that of (L)-host and (D)-PEA, and (D)-form of host gave mirror-like results, indicating the enantioselectivity of host for PEA enantiomers (Table S6). More interestingly, H_2SA could form complex with PEA by virtue of the achiral benzoic acid group, and the partial deprotonation of carboxylate group implying the strong binding affinity (Figs. S64–S65). Such interactions could well explain the high binding constant but low enantioselectivity of H_2SA. By comparing the energy of complexes, the largest energy difference is found for that of SA-Cd, implying that SA-Cd has better enantioselectivity for PEA enantiomer compared with serine and H_2SA ligand (Fig. 3d). Considering the polymer nature of SA-Cd, further calculations based on the single crystal periodical structures were performed using VASP (Figs. S66–S69). The results indicated that during recognition helical chains of SA-Cd could be maintained, only surface exposed –OH groups were able to form H-bonds with the $–NH_2$ group of PEA. The binding constants (Table S7) and binding energy (Table S8) in vacuum were also calculated, further confirming the high enantoselectivity of SA-Cd achieved upon constructing a free ligand into a coordination polymer.

4. Conclusions

In conclusion, two serine-based HCP enantiomers were explored as

Table 2
Comparison of literature results on PEA enantiomer recognition with this work.

Material	Method	Enantioselective factor	*ee*%	Ref
Chiral calixarene	QCM	1.03	/	Temel et al. (2019)
Binaphthalene boron-dipyrromethene	Fluorescence	1.40	/	Beer et al. (2001)
Metallosalalen chiral Cage	Fluorescence	2.87	17.1%	Dong et al. (2014)
Lipophilic peptide	Association constant	1.47	/	Mathew et al. (2000)
Binuclear Ni(II) Complex	Crystallization followed by HPLC	/	30.0%	Das et al. (2014)
Zinc bisporphyrinate	Circular dichroism	/	/	Fang et al. (2015)
Metallosalan chiral Cage	Adsorption followed by HPLC	/	14.6%	Xuan et al. (2012)
Chiral metallacycles	Fluorescence	3.90 ± 0.52	/	Dong et al. (2017)
Polyacetylene/Fe_3O_4 gels	Optical rotation	5.32	/	Liu et al. (2013)
Chiral calixarene	QCM	1.34	/	Ozcelik et al. (2019)
Tetraphenylethylene derived Schiff base	Fluorescence	2.50	/	Zhang et al. (2018)
Chiral boronic ester	Fluorescence	3.50	/	Jiao et al. (2014)
Chiral MOFs	Adsorption followed by HPLC	/	91.0%	Peng et al. (2014)
Chiral MOFs	QCM	2.20	/	Duan et al. (2015)
Organic polymer	HPLC	/	41.0%	Maeda et al. (2011)
Furo-fused BINOL	Fluorescence	2.97	/	Upadhyay et al. (2007)
SA-Cd enantiomers	QCM	2.89 ± 0.09	40.64 ± 2.91%	This work

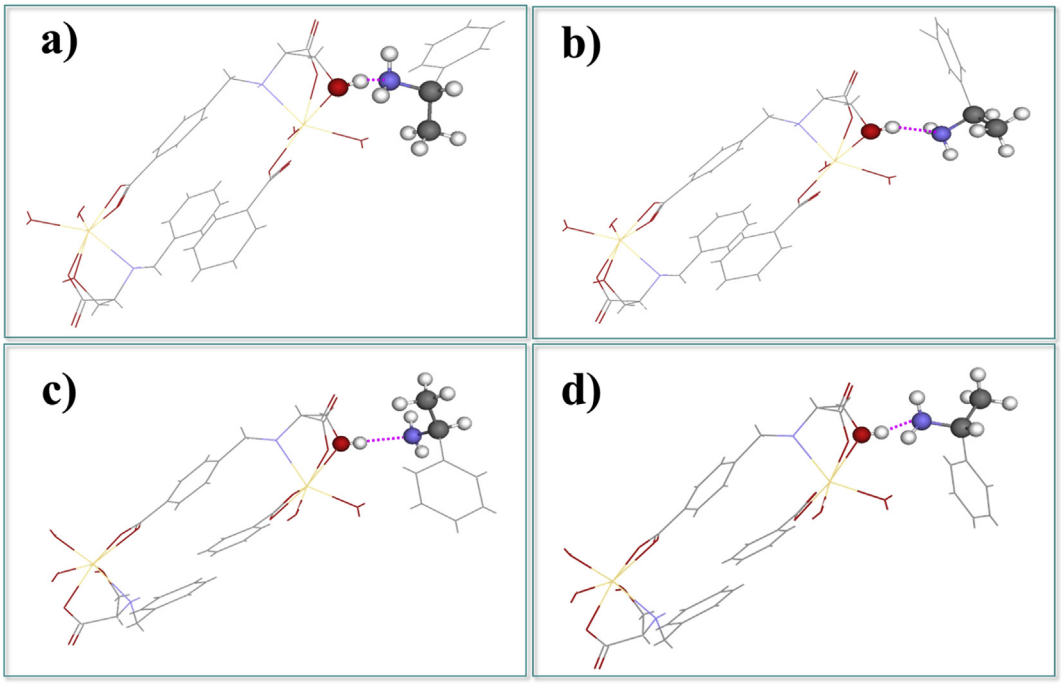

Fig. 4. Calculated local structures of the complexes formed by SA-Cd and PEA enantiomers. a) (L)-SA-Cd with (L)-PEA; b) (L)-SA-Cd with (D)-PEA; c) (D)-SA-Cd with (L)-PEA; d) (D)-SA-Cd with (D)-PEA.

enantioselective QCM sensors for four pairs of analyte enantiomers. SA-Cd exhibited the best enantioselectivity towards PEA enantiomers with an *ef* value of 2.89 ± 0.09. Control experiments indicate the positive role of forming coordination polymers in advancing the enantioselectivity. Mechanistic studies were carried out by comprehensive experiments and DFT calculations, and H-bonding effect between the surface exposed chiral –OH groups of SA-Cd and $–NH_2$ group of PEA is found to be the reason for the observed enantioselectivity. The major limitation of this work is the relative low activity in enantioselective adsorption/separation of racemic PEA, and this should be because of the non-porous structures of SA-Cd, which could only use the very limited surface groups for enantioselective application. This work demonstrates that constructing chiral molecules into HCP represents an effective way of promoting the enantioselectivity, and our future work will focus on the construction of porous homochiral frameworks with rigid chiral linkers, and more novel enantioselective sensors with promising applications shall be expected.

CRediT authorship contribution statement

Ming-Hua Xie: Formal analysis, Data curation, Writing - original draft. **Feng Cheng:** Software. **Ya Wang:** Investigation. **Bai-Xin Yao:** Investigation. **Wei Wang:** Resources. **Rong-Feng Guan:** Supervision. **Xiu-Li Yang:** Writing - review & editing, Supervision, Project administration.

Declaration of competing interest

The authors declare that they have no known competing financial interests or personal relationships that could have appeared to influence the work reported in this paper.

Acknowledgment

We thank the financial support of the National Natural Science Foundation of China (21775136, 21771158, 21301149, 21401160), the Natural Science Foundation of the Jiangsu Higher Education Institutions of China (17KJB150039), the Qing Lan Project, the Six Top Talents Program of Jiangsu Province (2018-XCL-063, 2019-XCL-097), the 333 Project of Jiangsu Province (BRA2019287), the Talent Project of Jiangsu Association for Science and Technology, Research Funds from Anhui Province Key Laboratory of Chemistry for Inorganic/Organic Hybrid Functionalized Materials, and Joint Open Fund of Jiangsu Collaborative Innovation Center for Ecological Building Material and Environmental Protection Equipments and Key Laboratory for Advanced Technology in Environmental Protection of Jiangsu Province (JH201821), and financial support from Yancheng Institute of Technology. We are very grateful to Prof. Chuan-De Wu of Zhejiang University for his help in single crystal analysis.

Appendix A. Supplementary data

Supplementary data to this article can be found online at https://doi.org/10.1016/j.bios.2019.111667.

References

Anand, R., Borghi, F., Manoli, F., Manet, I., Agostoni, V., Reschiglian, P., Gref, R., Monti, S., 2014. J. Phys. Chem. B 118, 8532–8539.
Beer, G., Rurack, K., Daub, J., 2001. Chem. Commun. 1138–1139.
Chankvetadze, B., 2004. Chem. Soc. Rev. 33, 337–347.
Cui, Y., Li, B., He, H., Zhou, W., Chen, B., Qian, G., 2016. Acc. Chem. Res. 49, 483–493.
Das, C.R., Sahoo, S.C., Ray, M., 2014. Cryst. Growth Des. 14, 3958–3966.
Dong, J., Zhou, Y., Zhang, F., Cui, Y., 2014. Chem. Eur J. 20, 6455–6461.
Dong, J., Tan, C., Zhang, K., Liu, Y., Low, P.J., Jiang, J., Cui, Y., 2017. J. Am. Chem. Soc. 139, 1554–1564.
Duan, H.-J., Yang, C.-X., Yan, X.-P., 2015. RSC Adv. 5, 30577–30582.
Frisch, M.J., Trucks, G.W., Schlegel, H.B., Scuseria, G.E., Robb, M.A., Cheeseman, J.R., Scalmani, G., Barone, V., Mennucci, B., Petersson, G.A., Nakatsuji, H., Caricato, M., Li, X., Hratchian, H.P., Izmaylov, A.F., Bloino, J., Zheng, G., Sonnenberg, J.L., Hada, M., Ehara, M., Toyota, K., Fukuda, R., Hasegawa, J., Ishida, M., Nakajima, T., Honda, Y., Kitao, O., Nakai, H., Vreven, T., Montgomery Jr., J.A., Peralta, J.E., Ogliaro, F., Bearpark, M., Heyd, J.J., Brothers, E., Kudin, K.N., Staroverov, V.N., Kobayashi, R., Normand, J., Raghavachari, K., Rendell, A., Burant, J.C., Iyengar, S.S., Tomasi, J., Cossi, M., Rega, N., Millam, J.M., Klene, M., Knox, J.E., Cross, J.B., Bakken, V., Adamo, C., Jaramillo, J., Gomperts, R., Stratmann, R.E., Yazyev, O., Austin, A.J., Cammi, R., Pomelli, C., Ochterski, J.W., Martin, R.L., Morokuma, K., Zakrzewski, V.G., Voth, G.A., Salvador, P., Dannenberg, J.J., Dapprich, S., Daniels, A.D., Farkas, Ö., Foresman, J.B., Ortiz, J.V., Cioslowski, J., Fox, D.J., 2013. Gaussian 09, Revision D.01. Gaussian, Inc., Wallingford CT.

Fang, X., Han, Z., Xu, C., Li, X., Wang, Y., Hu, C., 2015. Dalton Trans. 44, 12511–12515.
Heinke, L., Wöll, C., 2019. Adv. Mater., 1806324.
Jensen, K., Kim, K., Zettl, A., 2008. Nat. Nanotechnol. 3, 533–537.
Jiao, J., Wei, G., Li, F., Mao, X., Cheng, Y., Zhu, C., 2014. RSC Adv. 4, 5887–5892.
Kresse, G., Furthmüller, J., 1996. Phys. Rev. B 54, 11169–11186.
Kumar, J., Liz-Marzán, L.M., 2019. Bull. Chem. Soc. Jpn. 92, 30–37.
Liu, D., Chen, H., Deng, J., Yang, W., 2013. J. Mater. Chem. C 1, 8066–8074.
Liu, M., Zhang, L., Wang, T., 2016. Chem. Rev. 115, 7304–7397.
Mathew, B., Kuboyama, T., Nakamura, S., Takagi, M., 2000. Chem. Lett. 29, 1026–1027.
Ma, L., Abney, C., Lin, W., 2009. Chem. Soc. Rev. 38, 1248–1256.
Ma, W., Xu, L., Wang, L., Xu, C., Kuang, H., 2019. Adv. Funct. Mater. 29, 1805512.
Maeda, K., Kuroyanagi, K., Sakurai, S.-i., Yamanaka, T., Yashima, E., 2011. Macromolecules 44, 2457–2464.
Morris, R.E., Bu, X., 2010. Nat. Chem. 2, 353–361.
Mahadevi, A.S., Sastry, G.N., 2016. Chem. Rev. 116, 2775–2825.
Martell, J.D., Porter-Zasada, L.B., Forse, A.C., Siegelman, R.L., Gonzalez, M.I., Oktawiec, J., Runčevski, T., Xu, J., Srebro-Hooper, M., Milner, P.J., Colwell, K.A., Autschbach, J., Reimer, J.A., Long, J.R., 2017. J. Am. Chem. Soc. 139, 16000–16012.
Meng, X., Wang, H.-N., Song, S.-Y., Zhang, H.-J., 2017. Chem. Soc. Rev. 46, 464–480.
Mon, M., Ferrando-Soria, J., Verdaguer, M., Train, C., Paillard, C., Dkhil, B., Versace, C., Bruno, R., Armentano, D., Pardo, E., 2017. J. Am. Chem. Soc. 139, 8098–8101.
Ozcelik, E., Temel, F., Erdemir, S., Tabakci, B., Tabakci, M., 2019. J. Incl. Phenom. Macrocycl. Chem. https://doi.org/10.1007/s10847-019-00892-z.
Pan, M., Wu, K., Zhang, J.-H., Su, C.-Y., 2019. Coord. Chem. Rev. 378, 333–349.
Perdew, J.P., Chevary, J.A., Vosko, S.H., Jackson, K.A., Pederson, M.R., Singh, D.J., Fiolhais, C., 1992. Phys. Rev. B 46, 6671–6687.
Peng, Y., Gong, T., Zhang, K., Lin, X., Liu, Y., Jiang, J., Cui, Y., 2014. Nat. Commun. 5, 4406.
Pramanik, S., Zheng, C., Zhang, X., Emge, T.J., Li, J., 2011. J. Am. Chem. Soc. 133, 4153–4155.
Pu, L., 2012. Acc. Chem. Res. 45, 150–163.
Sethy, R., Kumar, J., Métivier, R., Louis, M., Nakatani, K., Mecheri, N.M.T., Subhakumari, A., Tomas, K.G., Kawai, T., Nakashima, T., 2017. Angew. Chem. Int. Ed. 56, 15053–15057.
Staszak, K., Wieszczycka, K., Marturano, V., Tylkowski, B., 2019. Coord. Chem. Rev. 397, 76–90.
Slater, B., Wang, Z., Jiang, S., Hill, M.R., Ladewig, B.P., 2017. J. Am. Chem. Soc. 139, 18322–18327.
Temel, F., Erdemir, S., Tabakci, B., Akpinar, M., Tabakci, M., 2019. Anal. Bioanal. Chem. 411, 2675–2685.
Upadhyay, S.P., Pissurlenkar, R.R.S., Coutinho, E.C., Karnik, A.V., 2007. J. Org. Chem. 72, 5709–5714.
Wanderley, M.M., Wang, C., Wu, C.-D., Lin, W., 2012. J. Am. Chem. Soc. 134, 9050–9053.
White, J.A., Bird, D.M., 1994. Phys. Rev. B 50, 4954–4957.
Xuan, W., Zhang, M., Liu, Y., Chen, Z., Cui, Y., 2012. J. Am. Chem. Soc. 134, 6904–6907.
Yang, X.-L., Xie, M.-H., Zou, C., Sun, F.-F., Wu, C.-D., 2011a. CrystEngComm 13, 1570–1579.
Yang, X.-L., Xie, M.-H., Zou, C., Wu, C.-D., 2011b. CrystEngComm 13, 6422–6430.
Yang, X.-L., Wu, C.-D., 2014. CrystEngComm 16, 4907–4918.
Yang, F., Xu, G., Dou, Y., Wang, B., Zhang, H., Wu, H., Zhou, W., Li, J.-R., Chen, B., 2017. Nat. Energy 2, 877–883.
Yi, F.-Y., Wang, Y., Li, J.-P., Wu, D., Lan, Y.-Q., Sun, Z.-M., 2015. Mater. Horiz. 2, 245–251.
Yoshinari, N., Konno, T., 2018. Bull. Chem. Soc. Jpn. 91, 790–812.
You, L., Zha, D., Anslyn, E.V., 2015. Chem. Rev. 115, 7840–7892.
Zuo, Z., Cong, H., Li, W., Choi, J., Fu, G.C., MacMillan, D.W.C., 2016. J. Am. Chem. Soc. 138, 1832–1835.
Zhang, G.-W., Li, P.-F., Meng, Z., Wang, H.-X., Han, Y., Chen, C.-F., 2016. Angew. Chem. Int. Ed. 55, 5304–5308.
Zhang, F.-M., Dong, L.-Z., Qin, J.-S., Guan, W., Liu, J., Li, S.-L., Lu, M., Lan, Y.-Q., Su, Z.-M., Zhou, H.-C., 2017. J. Am. Chem. Soc. 139, 6183–6189.
Zhang, X., Yu, Q., Chen, S., Dai, Z., 2018. New J. Chem. 42, 4045–4051.
Zhao, Y.-W., Wang, Y., Zhang, X.-M., 2017. ACS Appl. Mater. Interfaces 9, 20991–20999.